



A new electro-osmotic pump based on silica monoliths

Ping Wang, Zilin Chen, Hsueh-Chia Chang *

*Center for Micro-fluidics and Medical Diagnostics, Department of Chemical and Biomolecular Engineering,
University of Notre Dame, Notre Dame, IA 46556, USA*

Received 20 October 2004; received in revised form 17 February 2005; accepted 16 March 2005

Available online 24 May 2005

Abstract

A high-pressure electro-osmotic (EO) micro-pump fabricated by a sol-gel process is shown to be potentially effective as a fluid-driving unit on chip-scale analytical systems. A silica monolithic matrix with a morphology of micron-scaled through pores was synthesized within the 100 μm inner diameter (i.d.) fused-silica capillary of the micro-pump. The monolith bonds directly with the capillary wall such that frits with large pressure loss are unnecessary. This pump uses electro-osmotic flow to propel liquid solution with no moving parts. The Nafion® housing design in the cathode chamber prevents flow leakage into the electrode reservoir from the flow channel and hence maximizes the pressure build-up. It also eliminates electrolytic bubble interference from the flow channels and provides ionic channels for current penetration simultaneously. As the monolith is silica-based, this pump can be used for a variety of fluids, especially for organic solvents, such as acetonitrile and methanol, without swelling and shrinking problems. The maximum flow rate and maximum pressure generated by the 100 μm i.d. monolithic pump are 2.9 μL/min and 3 atm for deionized water at 6 kV applied voltage. These results indicate that the pump can provide sufficient pressure and flow for miniaturized HPLC and micro-total-analysis systems (μ-TAS). A simple universal pressure pump curve collapses the data for a variety of working fluids and voltage.

© 2005 Elsevier B.V. All rights reserved.

Keywords: Micro-pump; Electro-osmosis; Electrokinetic; Silica; Monolith

1. Introduction

Miniature systems for chemical and biological analysis have attracted considerable attention in recent years due to their portability, reduced consumption of samples and reagents and less manual intervention. [1,2] When devices are miniaturized to micro-scale, the smaller channels and the larger capillary pressure across menisci [3] in miniature systems require imbedded micro-pumps that can produce a substantial pressure. A number of such micro-pumps have been designed and built using micro-fabrication technologies. Generally, they can be divided into two categories [4,5]: (i) displacement (mechanical) pumps and (ii) dynamic pumps. The former often involves moving parts, such as oscillating membranes, check valves or micro-turbines, and typically cannot provide enough pressure to overcome the

high hydrodynamic resistance and capillary pressures of miniature systems. Although many pumps can load and drive liquids in a wide range of flow rates, only electro-osmotic flow (EO) pumps which belong to the second category are capable of generating high pressure (typically greater than 1 atm). Unlike mechanical pumps with moving parts, which are prone to frictional wear, other notable advantages of EO pumps are that they are cheap and easy to be fabricated. EO pumps also offer precise delivery of small amounts of fluids with strategically placed electrodes. The electrodes can be separated from the flow channels by applying conductive membranes so that undesirable electrolytic products, such as gas bubbles, can be released into surrounding environment without invading into the flow channels [6–8].

Although EO phenomena were discovered nearly 200 years ago [9], its application to miniature analysis systems has only generated interest in the last few years when a means of generating substantial pressure is realized for EO flow. Proetorius et al. [10] and Theeuwes [11] first proposed this

* Corresponding author.

E-mail address: hchang@nd.edu (H.-C. Chang).

concept for high-speed liquid chromatography. Paul et al. [12] reported that a capillary EO pump packed with silica micro-particles can produce a pressure of 10 atm and a flow rate of 0.03 $\mu\text{L}/\text{min}$ at 1.5 kV applied voltage. The high pressure is produced by the small pores of the packing-hydrodynamic resistance. Zeng et al. [13,14] employed two polymer frits to sandwich a layer of densely packed silica micro-particles in a cube-shape acrylic frame (transverse dimension \sim 15 mm) which can provide flow rates as high as 0.8 mL/min at 1 atm backpressure. However, beads packing EO pumps suffer from drawbacks, such as tedious packing procedures and the necessity for frits to anchor them at specific locations. Moreover, considerable pressure drop can occur across the frits (\sim 50% of the total pressure drop) [13]. This pressure loss significantly reduces the efficiency of the pump as it cannot be utilized for the external load.

Chen and Santiago [15] reported a parallel-plate pump which does not use interior packing. It uses a row of high aspect ration channel etched in glass by a standard micro-fabrication technology. This planar EO pump can be integrated with other chip-level micro-systems. However, its relatively large width reduces the hydrodynamic resistance necessary to produce very high pressure. Recently, Tripp et al. [16] reported an *in situ* preparation of a porous polymer monolith as a pump matrix by polymerization from liquid precursors including monomers, cross-linker, free radical initiator and porogenic solvents. Post-polymerization process of grafting of ionizable monomers to the monolith is essential to render considerable surface charge densities. When working with organic solvents, polymer monoliths tend to swell or even clog flow channels.

We have reported an ac electrokinetic micro-pump and micro-mixer design based on ac Faradaic polarization of fabricated electrodes [17]. The ac polarization produces far less net reaction products than a dc pump (zero net reaction product from a perfectly symmetric reaction). The Arrhenius exponential scaling of Faradaic polarization with respect to voltage also produces higher polarization than electrodes coated with dielectric films that do not allow Faradaic reactions. However, as the bare electrodes are imbedded in the flow channel, ions and bubbles released from the electrode Faradaic reactions cannot be isolated from the flow channel. Consequently, the ac pump must still operate at a relatively low voltage (<20 V) to minimize net reaction product generation and hence cannot produce high pressure.

Chen (one of present author) et al. reported that monolithic silica columns have been well used for capillary electrochromatography, micro-liquid chromatography [18–20] and enzyme micro-reactor [21]. We propose silica-based monolith as a very promising structure for dc EO flow generation. The chemistry of silica is well known and the material has an intrinsic ability to generate a strong EO flow due to the presence of ionizable silanol groups at its surface. In fact, the silica monolith has a bimodal pore distribution [22] whose nano-porous structure will be shown

to produce a higher charge density than regular fused-silica glasses and non-porous silica particles. The silanol groups at the fused-silica capillary wall can be easily cross-linked to the silica monolith network to assure secure linkage. Frits are unnecessary and thus the efficiency of the pump can be improved. Swelling and clogging are absent rather than polymer monolith when organic solvents are used as working fluids. This pump was also proved to be effective and robust as a fluid-driving unit on chip-scale analytical systems in a forthcoming paper [23]. In that example, the pump was integrated with a micro-electrochemical sensor that can perform a micro-fluid injection analysis (μ -FIA).

This report presents the first fabricated EO micro-pump that uses the silica monolith. We also employ a Nafion® cathode housing design that can prevent the invasion of undesirable electrolytic products like bubbles into the flow channel in addition to avoid flow leakage. A high-pressure pump is demonstrated within a 100 μm capillary and its pressure curve is accurately captured by a simple theory for a variety of working fluids, including electrolyte buffer solutions, deionized water (DI), acetonitrile and methanol. The efficiency of the pump is shown to be largest for low-conductivity fluids.

2. Theory of EO pumping

Electro-osmosis is a common technique for pumping fluids. If the wall of capillary or micro-channel has electric charges, as most surfaces do, an electric double layer of counter ions will spontaneously form at the wall [24]. In the case of a silica monolith, the main source of surface charges comes from deprotonation of silanol groups which produce a negatively charged surface at neutral pH. When a tangential electric field is applied, ions in the double layer suffer a Coulombic force, called the Maxwell force, and move towards the electrode of opposite polarity. This creates motion of the fluid near the wall and transfers momentum via viscous forces into the bulk. If the channel is not connected to any frictional load, the velocity profile is uniformly flat across the entire channel as shown on the lower left in Fig. 1 (double layer region is exaggerate for clarity). This flow exists between the two electrodes that supply the tangential field. However, if the EO pumps work against a hydrodynamic load with significant viscous dissipation, a backpressure is generated to reduce the flow within the pump channel such that the flow rate is the same inside the pump channel and the downstream load channel. As a result, a “frustrated” flow pattern forms within the pump channel for which the fluid along the center of the channel moves at a different velocity from that at the walls as shown in Fig. 1. In the most extreme case, the velocity can even change direction across the channel for this mixed flow pattern.

Rice and Whitehead [25] derived the velocity profile for the frustrated flow in a capillary of radius α under a tangential

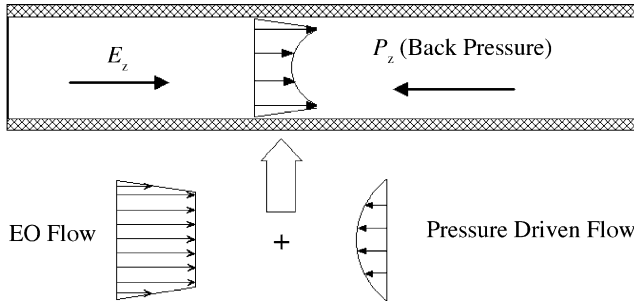


Fig. 1. Frustrated flow of EO pump in a capillary (double layer region is exaggerated for clarity): in EO flow, mobile ions in the double layer are driven by an external electric field. These moving ions supply viscous drag to the bulk liquid and the flow profile is flat as shown on the lower left. The backpressure is exerted by external load and the flow profile is parabolic as shown on the lower right. The resulting velocity flow profile is a linear combination of these two.

electrical field E_z ,

$$u(r) = \frac{P_z}{4\mu}(a^2 - r^2) - \frac{\varepsilon E_z \zeta}{\mu} \left(1 - \frac{\phi(r/\lambda)}{\zeta}\right) \quad (1)$$

where ε , μ and ζ denote the dielectric permittivity, viscosity of the working fluids and the zeta potential of silica monolith surface. The pressure gradient along the flow direction is P_z while ϕ is the potential in the capillary, which is a function of the radial coordinate r scaled by the double layer thickness. The double layer thickness λ is also known as the Debye shielding distance. For an aqueous solution of a binary symmetric electrolyte, the double layer thickness is

$$\lambda = \left(\frac{\varepsilon RT}{2F^2 z^2 c_\infty}\right)^{1/2} \quad (2)$$

where c_∞ is the counter ion concentration of bulk solution. It can be seen that λ decreases inversely as the square root of the ion concentration. The double layer thickness was estimated in Table 1 according to the bulk conductivity for a variety of working fluids to be used in our pump [26]. Bulk region was considered to be infinite large.

In order to get a closed-form analytical solution of the potential profile across the capillary, that is convenient for data scaling, a Debye–Hückel approximation can be made such that the potential drop from the centerline to the surface is assumed to be small compared to the thermal noise, $ze\phi/kT \ll 1$. This assumption generates the non-dimensional

potential as

$$\phi\left(\frac{r}{\lambda}\right) = \zeta \frac{I_0(r/\lambda)}{I_0(a/\lambda)} \quad (3)$$

where I_0 is the zero-order modified Bessel function of the first kind.

Zeng et al. [13] extended the above analysis for an open capillary to that for a porous medium and obtained the flow rate

$$Q = \frac{\psi P_z A a^2}{8\mu\tau} - \frac{\psi\varepsilon\zeta E_z A}{\mu\tau} \left(1 - \frac{2\lambda I_1(a/\lambda)}{a I_0(a/\lambda)}\right) \quad (4)$$

The cross-section area of the porous medium in consideration is A and the tortuosity τ is defined as $(L_e/L)^2$, where L_e is the effective channel length and L is the true channel length of the channel containing the porous medium. The porosity ψ is the ratio of the void volume to the total volume of the porous medium. The maximum pressure can be derived by setting Eq. (4) to zero which is the case of closed channels, while the maximum flow rate can also be obtained at zero backpressure,

$$\Delta P_{\max} = -\frac{8\varepsilon\zeta L E_z}{a^2} \left(1 - \frac{2\lambda I_1(a/\lambda)}{a I_0(a/\lambda)}\right) \quad (5)$$

$$Q_{\max} = -\frac{\varepsilon\psi\zeta A E_z}{\tau\mu} \left(1 - \frac{2\lambda I_1(a/\lambda)}{a I_0(a/\lambda)}\right) \quad (6)$$

Combining Eqs. (5) and (6), a linear pump curve is obtained for the flow rate and pressure of an EO pump working against a load,

$$\frac{\Delta P}{\Delta P_{\max}} + \frac{Q}{Q_{\max}} = 1 \quad (7)$$

This linear relationship is the result of linear flow rate associated with EO flow and pressure driven flow. Eqs. (5) and (6) can also be combined to give the ratio between Q_{\max} and ΔP_{\max} ,

$$\frac{Q_{\max}}{\Delta P_{\max}} = \frac{A}{8\mu L} \frac{\psi a^2}{\tau} \quad (8)$$

Eq. (8) can be used to determine the effective pore size of a complicated or irregular structure, such as beads packing or monoliths. Eq. (7), on the other hand, is only valid if bubbles are absent in the pump and if ions generated by the electrodes have not significantly altered the electrokinetic properties of the monolith. Hence, collapse of the data by this equation, especially at the high pressure/low flow rate limit when advection is too low to remove the offending bubbles or ions, would be a good indication that both are absent.

Table 1
Bulk conductivity and estimated double layer thickness (for 1:1 type electrolytes)

Examples	Bulk conductivity ($1/\Omega \text{ m}$)	Ionic strength I_M (mM)	Double layer thickness (nm)
pH buffers, such as Tris–EDTA	$\sim 10^{-1}$ $\sim 10^{-2}$	~ 10 ~ 1	~ 3 ~ 10
DI water	$\sim 10^{-4}$	$\sim 10^{-2}$	~ 100
Acetonitrile	$\sim 10^{-6}$	$\sim 10^{-4}$	~ 1000

Eq. (5) indicates that the high hydrodynamic resistance offered by a small pore size is responsible for the high pressure, while Eq. (6) indicates a large cross-section area is desirable for a large flow rate. Both are obviously desirable but they clearly occur at different limits. An optimum trade-off is then a bundle of parallel micro-channels with small pore size. However, the pore size cannot be smaller than the double layer thickness, as polarization, Maxwell force and flow would all diminish significantly. Hence, the ideal structure is a porous medium with parallel pores whose radius is comparable to the double layer thickness. A monolithic matrix offers such a structure with a small pore radius that approaches the double layer thickness of some polar organic liquids.

Pumping efficiency is another important measure for liquid-driving devices. EO pumps are very inefficient if the working fluid is relatively conductive. EO flow relies on a net Maxwell force on the liquid when an electric field is applied to a region containing mobile ions which have a collective net charge. In EO flow, this net charge exists only within the surface double layer, which is typically around several nanometres in thickness for mostly used electrolyte buffer solutions. The efficiency of EO pump is hence much lower (by an order of magnitude or more) than mechanical pumps as its body force and hydrodynamic shear are confined to the thin double layer rather than across the entire channel. This confinement leads to extremely large wall shear and viscous dissipation. Another significant energy dissipation is electrical Joule heating. Due to neutrality of the bulk, the net Maxwell force is zero there as the drag force supplied by the positive ions is cancelled by that by negative ions. The ion motion, however, still effect Joule heating which is a serious problem for conductive electrolyte solution.

The pump efficiency can be defined as ‘useful’ work over total power consumption. In the case of EO pump, the useful work is the pressure work that the working fluid can supply. We can hence define the thermodynamic efficiency as

$$\eta = \frac{\Delta PQ}{VI} \quad (9)$$

The useful pressure work is defined as ΔPQ while the total power consumption is VI . As a reference point, the total power consumption of a mechanical pump whose moving parts suffer no friction loss is also ΔPQ . The efficiency of a frictionless mechanical part is hence unity. The efficiencies of actual micro-mechanical pumps are rarely reported in the literature. A small number of thermodynamic efficiency of micro-pump has been collected and estimated by Laser and Santiago [5]. For example, the typical efficiency of electromechanical conversion in piezoelectrics is typically between 10 and 30% (excluding the finite efficiency of the voltage conversion and ac voltage control). We expect them to be related to the size of the moving parts and their load (viz. their frictional wear).

The total current, I , is the sum of bulk conduction current, I_b , in the electroneutral portion in the pore and surface current, I_s , which is carried by the motion of ions inside the

charged double layer. If the double layer is much thinner than pore diameter, most of the current is carried by I_b in the bulk, where a net Maxwell force that drives the fluid does not exist. The efficiency is hence expected to be much lower than macroscopic mechanical pumps in this case. If the double layer is comparable to or exceeds the pore size, I_s might dominate over I_b and the efficiency could be higher and may approach that of macro-mechanical pumps. We shall utilize the above theory to characterize our high-pressure dc EOF pump and, in fact, to produce a universal pump curve for a variety of working fluids in the silica monolith when the double layer approaches but does not exceed the pore radius. The efficiency remains low compared to macro-mechanical pumps. However, the backpressure is much higher than most reported micro-mechanical pumps and other EOF pumps of comparable channel cross-section area.

3. Fabrication and characterization

3.1. Reagents

Tetramethoxysilane (TMOS) and poly(ethylene glycol) (PEG, $M_w = 10,000$) were obtained from Sigma–Aldrich (USA) and used without further purification. Disodium ethylenediamine tetraacetate (EDTA), tris(hydroxymethyl) aminomethane (Tris), sodium hydroxide, hydrochloric acid and acetic acid were purchased from Fisher Scientific (USA). All solutions were prepared using DI water.

3.2. Pretreatment of capillaries

Fused-silica capillaries were obtained from Polymicro Technologies Inc. (Phoenix, AZ). Prior to use, silica capillaries were first flushed with 1 M sodium hydroxide (30 min), followed with 0.1 M hydrochloric acid (30 min) and then with DI water (30 min) at 20 °C. Finally, the capillaries were flushed with acetone (30 min) and put into oven at 105 °C for 2 h to remove all liquids inside them. These pretreatments can eliminate impurities inside the capillary and activate the inside wall for further sol–gel reaction.

3.3. Preparation of silica-based monolithic matrix

The monolithic silica matrix was prepared by referring to the procedures of Refs. [18–22] with some modifications. Briefly, 0.5 mL of 0.01 M acetic acid, 54 mg of PEG and 0.2 mL of TMOS were mixed in a micro-liter size vial bottle. The solution was stirred for about 30 min in an ice–water bath (0 °C). When all PEG has dissolved and a transparent and single-phase solution was observed, the solution was then introduced into a 40 cm long capillary (100 μm i.d.) using a regular syringe. Two ends of the capillary were then connected with a Teflon® tube (Alltech, IL) to form a circle and then placed in a 40 °C oven for 12 h. The Teflon® connector was removed and the whole capillary was heated with

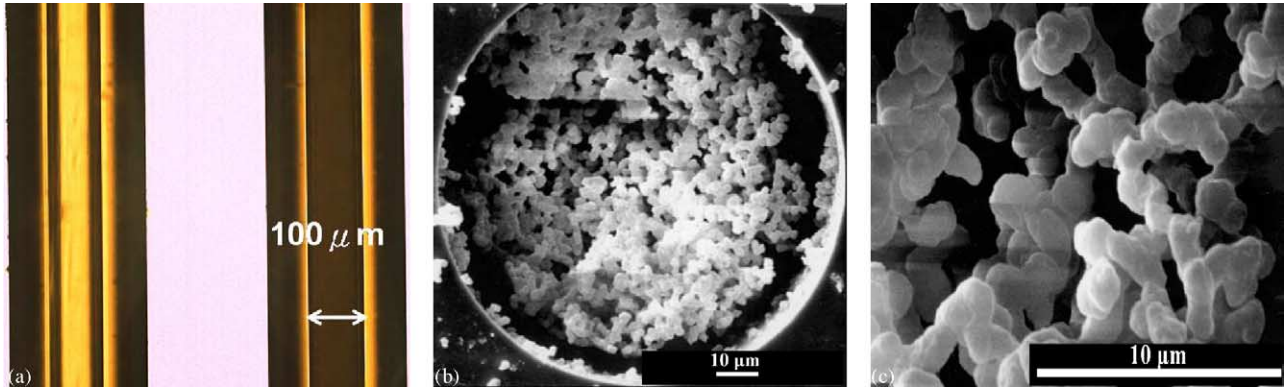


Fig. 2. Monolithic matrix inside the capillary. (a) Comparison images of open capillary (on the left) and the one with the monolithic matrix inside (on the right). The magnification is 20×. (b) SEM image of the cross-section with magnification of 1000×. The bar on the bottom denotes 10 μm. (c) SEM image of the same capillary with a magnification 5000×. The bar on the bottom denotes 5 μm.

a programmed temperature ramp. While the temperature was increased from 40 to 300 °C at a rate of 1 °C/min, it was soaked for 4 h at 80, 120, 180 and 300 °C, respectively. Finally, the capillary was cooled down to room temperature at a rate of 1 °C/min. Fig. 2(a) compares the images of an empty capillary (on the left side) and a monolithic matrix (on the right side) using an inverted Olympus IX71 microscope (USA). A homogenous monolithic matrix was observed though visualization. The capillaries with monolithic inside were checked to ensure integrality from one end till the other end prior to use. Fig. 2(b) shows a scanning electron microscope (SEM) image of the monolith. Many micro-through pores formed inside the silica monolithic matrix. Fig. 2(c)

is a magnified image of these pores, we can estimate the diameter of the micro-pores to be around 3–5 μm. It was verified in our earlier characterization [22] that there are many nano-size mesopores in the silica skeleton which makes it distinct from its counterpart of non-porous beads. We believe that high surface charge density can produce high zeta potential. The extremely porous structure of our silica monolith will have more “defective” sites than regular silica beads on its surface and hence more ionizable silanol groups can be generated. Although the role of the nano-pores will not be scrutinized in this report, we suspect they are responsible for the observed high charge density to be reported subsequently.

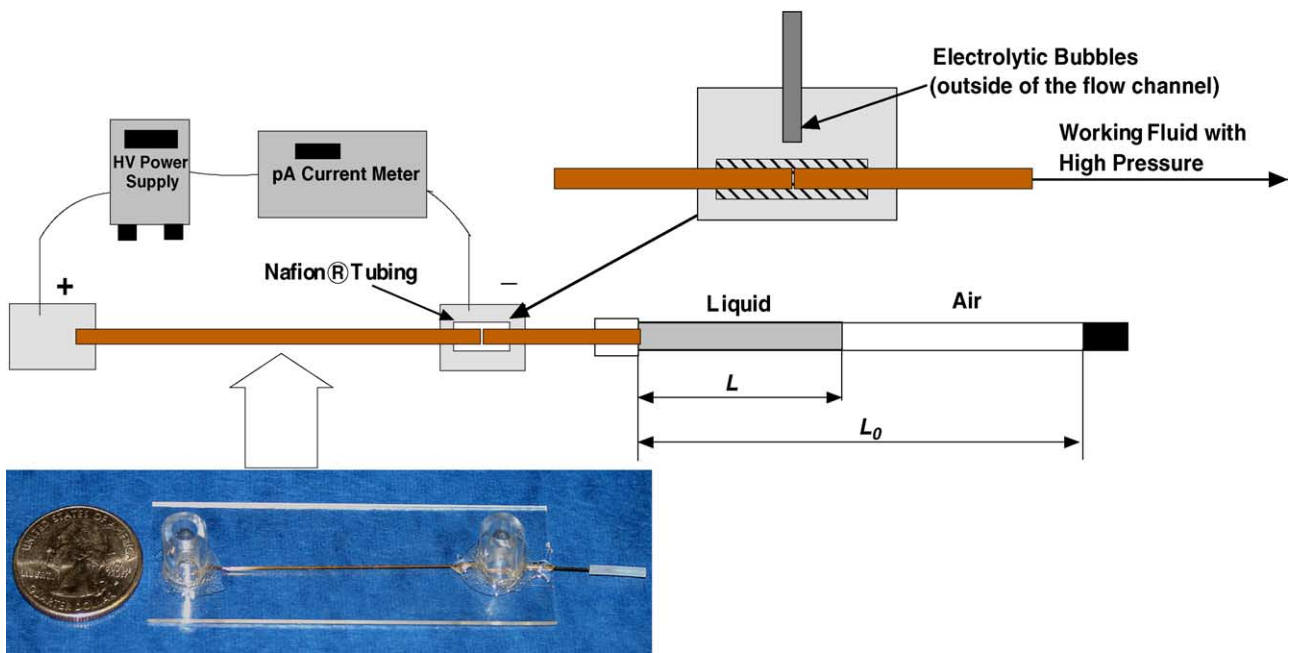


Fig. 3. Schematic of the assembled pump and the characterization setup. The test tube (300 μm i.d.) (dead-end) is connected to the outlet of the pump. Both flow rate and counter pressure are measured simultaneously. The solubility of the gas in the liquid is neglected here. The flow rate $Q = A dL/dt$, A is the cross-section area and L is the displacement of the meniscus. The counter pressure is $P = P_0 L_0/(L_0 - L)$ and $\Delta P = P - P_0$, where P_0 is 1 atm.

3.4. Fabrication of micro-pump

Fig. 3 shows a schematic of the assembled micro-pump. The monolithic capillary was mounted on a glass slide as shown in the bottom of **Fig. 3**. A US quarter was put near the pump to denote the real scale. A 6 cm long capillary with monolithic silica matrix inside was connected to another open capillary by a Nafion® tube membrane (Perma Pure, NJ) as shown on the upper right of **Fig. 3**. Nafion® is a conductive polymer (i.e. a charge-selective salt bridge) that permits diffusive and electrophoretic transport of ions. A small amount of epoxy glue was applied at two ends of the tube to strengthen the connection. Two pieces of PVC tubing (5 mm i.d.) were cut and glued on the two ends of the monolithic capillaries used as fluid reservoirs. Nafion® membrane plays several roles here. It can act both as a liquid junction unit and as an interface that separates bubbles generated by electrolytic reaction from the flow channels. The operation electric current in our experiment is very small (μA – nA) so that concentration polarization near the Nafion® surface can be neglected. Bubble generation reaction is fatal for micro-channel flow. Once gas bubbles invade into the channel, they have been shown to increase the effective viscosity of liquid dramatically due to the large capillary pressure across the meniscus—about 1 atm across a single meniscus in a micron-sized capillary [3,27]. The bubbles can also aggregate and block the electrical pathway. The conductive proton permeable Nafion® membrane prevents bubble invasion into the channel but allows electrical current penetration to sustain electrolytic reaction on the cathode electrode which is outside of the flow channel. More importantly, the membrane prevents flow leakage into electrode reservoir and hence holds the hydrodynamic pressure created by EO flow inside the capillary.

3.5. Characterization of the micro-pump

Tris–EDTA buffer, DI water, HPLC-grade acetonitrile and methanol/water mixture have been used as working fluids. The right side of **Fig. 3** shows the setup used for measuring the EOF of micro-pumps [15]. A HCZE-30PN025-LD high-voltage power supply (Matsusada Precision Device, Tokyo, Japan) was used to power the pump. The outflow was directed to a dead-end capillary to compress the internal air column. A relative large i.d. capillary (300 μm) was used to conduct pressure drop/flow rate measurements. The reason of that is to reduce the advanced speed of the meniscus by almost a factor of 10 ($(300/100)^2$) so that every date are close to their steady state values. The whole measurement usually took about 5–10 min. The position of the front meniscus was recorded optically to provide flow rate and pressure information. The electrical current passing through the capillary can be recorded by the current meter integrated in the power supply. Because the conductivity of DI water, acetonitrile and methanol/water mixture are very low and the current they carry is below the resolution of an integrated current meter ($>1 \mu\text{A}$), a pA meter (4140B, Hewlett-Packard) was linked

to the circuit to measure the current. Flow rate without back-pressure was measured by weighing the pumped fluid using an analytic weight scale (Sartorius, NY). The current with flow and without flow are dramatically different. We suspect that a large charge layer builds up at the Nafion membrane without flow due to a streaming potential effect. This charge build-up greatly reduces the current to the electrode. The charge build-up is presumably removed by the flow but even then, the current only reaches a steady state value after a 30 s transient. It is this steady value that is recorded.

4. Results and discussion

We do not visibly observe bubbles in either the electrode reservoir or the pump channels for all the working fluids and voltages reported. Measurements of pH over half an hour also indicate that the ions generated at the electrode have not invaded into the pump channel. We shall verify this absence of undesirable reaction products by collapsing our data with the theory of Section 2.

Fig. 4 shows the measured current versus voltage for an open and a monolithic capillary using a very conductive Tris–EDTA buffer solution with a conductivity of 54 mS/m. This electrolyte solution was chosen to reduce double layer thickness and hence reduce the effects of advective current from EO flow [28]. Both capillaries were 100 μm in diameter and 6 cm in length. The resistance ratio between the two is 0.4 which is the combined effects of porosity and tortuosity. Due to the considerably porous structure of the monolithic matrix shown in **Fig. 3(b and c)**, we assume that the tortuosity τ of the through pores to be around unity and attribute the resistance ratio only to porosity.

The measured current–voltage correlations for low-conductivity liquids, such as DI water, acetonitrile and methanol/water mixture, are shown in **Fig. 5**. These three liquids were chosen because of their wide applications in

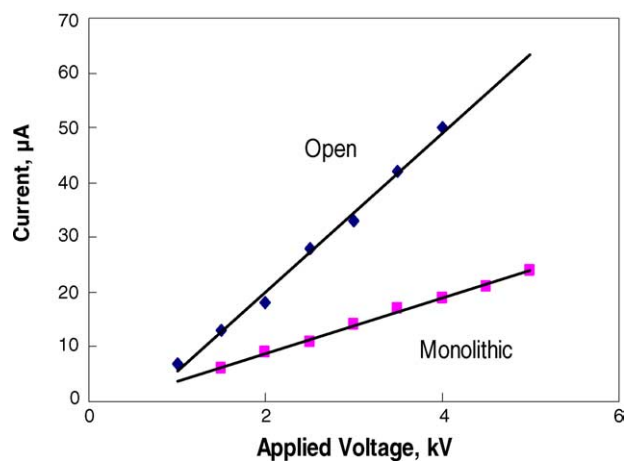


Fig. 4. The applied voltage and measured steady-state current of the monolithic pump and an open capillary. The EDTA–Tris buffer is used with a conductivity of 54 mS/m.

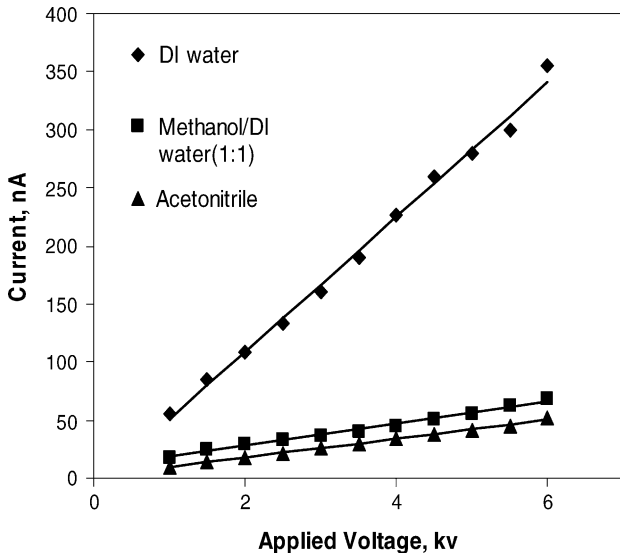


Fig. 5. Current vs. applied voltage for DI water, acetonitrile and methanol/water mixture. Because of the thick double layer of acetonitrile and methanol, the current is mainly carried by the surface current.

μ -TAS and micro-fuel cells. The measurements were conducted without backpressure when there is no downstream hydrodynamic load. Because of the low liquid conductivities, the double layer layers are not negligibly thin. The pores hence can be charged and advection current can be significant [28,29]. For acetonitrile and methanol/water mixture, the conductivities are as low as 10^{-6} S/m from Table 1 and the double layers thickness is around 1 μ m. The pore size of monolithic matrix is around 4 μ m hence the thicker double layers can span the narrower pores. The large difference (factor of 7) in conductivity between DI and a 1:1 DI/methanol mixture is because the values here represent effective conductivity inside a monolithic matrix.

We measured the pump curve of flow rate versus back-pressure using Tris-EDTA buffer, DI water and acetonitrile at 4–6 kV applied voltage. The pump curves for DI water and acetonitrile are shown in Figs. 6 and 7 and they exhibit linear scaling between backpressure and flow rate with identical slope as is consistent with Eq. (7). The only exception is the pump curve for acetonitrile at 6 kV, which has a 50% higher slope than that for the two lower voltages. Nischang and Tallarek also observed similar non-linear EO effects using very low-conductivity fluids and attributed this to EO of the second kind [30,31]. For DI water, the extrapolated maximum pressure and flow rate at 6 kV are about 3.1 atm and 2.9 μ L/min, respectively. This maximum pressure is high for the small pump channel cross-section area provided by the 100 μ m capillary. Because the flow rate is linearly dependent on the load pressure in the manner described by Eq. (7), the maximum pressure work ΔPQ occurs at the middle point of the pump curves in Figs. 6 and 7, where $\Delta P = \Delta P_{\max}/2$ and $Q = Q_{\max}/2$, which is the optimum operating condition with regard to thermodynamic efficiency. The current in the circuit for DI water is measured to be 150 nA at 6 kV and hence

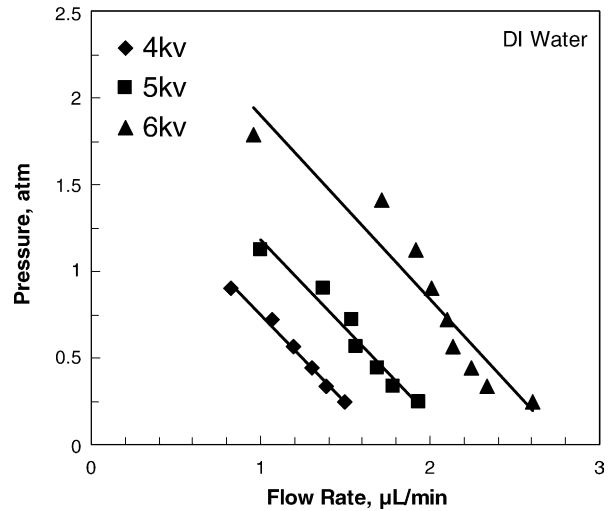


Fig. 6. Pressure vs. flow rate pump curves for the EO pump at different applied voltages of 3, 5 and 6 kV, respectively. Working fluid: DI water with conductance of 3.0×10^{-4} S/m.

the efficiency is 0.4%. The maximum electrical power consumption is 1.8 mW. From Eq. (8), the effective pore diameter can be calculated as 4 μ m which is also consistent with the SEM image of Fig. 2. From Table 1, the double layer thickness of DI water is around 0.1 μ m which is much smaller than channel pore size; hence, we can use the thin double layer approximation of Eq. (6) to calculate the zeta potential of silica monolith. The zeta potential for DI water is -190 mV which is higher than -100 mV of non-porous silica beads reported in the literature [13]. We attribute this high zeta potential to the bimodal porous structure of monolith which has a high charge density because of the high surface area to volume ratio of the nano-pores.

The extrapolated maximum flow rate and maximum pressure for the acetonitrile pump curve at 6 kV in Fig. 7 are

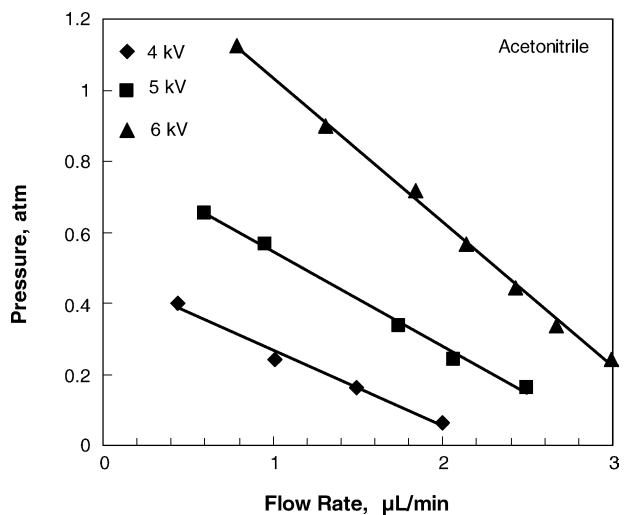


Fig. 7. Pressure vs. flow rate pump curves of the EO pump at different applied voltages of 3, 5 and 6 kV, respectively. Working fluid: acetonitrile with conductance of 1.0×10^{-6} S/m.

3.3 $\mu\text{L}/\text{min}$ and 1.5 atm, respectively. A lower backpressure is obtained compared to DI water as the lower conductivity allows for less power input. However, the efficiency is higher. At the optimum operating point at one half of these values, the current was measured to be 20 nA, and the corresponding efficiency 2.2% which is six times higher than that of DI water. It is still small compared to macroscopic mechanical pumps but may approach that of micro-mechanical pumps. The maximum power consumption at this optimum operating point is 0.3 mW. The higher efficiency and lower power consumption of acetonitrile is mainly due to its low conductivity. The resulting thick double layers under such low conductivity will occupy part of the flow channel space. The zeta potential for acetonitrile is 180 mV which is roughly the same as that for DI water. The EDTA–Tris buffer was also used as a working fluid. The current at the optimum condition for this fluid is measured to be 6 μA . Maximum flow rate and maximum pressure are 2.4 $\mu\text{L}/\text{min}$ and 3.4 atm at 6 kV applied voltage. The efficiency is as low as 0.012% and power consumption is 36 mW for this high-conductivity fluid. The efficiency is two orders of magnitude lower than that of acetonitrile. However, the higher conductivity produces a larger backpressure at comparable voltages. Nevertheless, to reduce the current and to enhance the efficiency of the pump, the pore size should be reduced to that of the double layer thickness for this strong electrolyte. As small as the pores of the silica monolith, they have yet to reach the double layer thickness of most working fluids.

To verify that our data are in agreement with the theory in Section 2, we scaled the pressure build-up and flow rate for each set of data by its measured ΔP_{\max} and Q_{\max} to obtain the normalized pump curve of Fig. 8. The observed excellent collapse indicates that undesired electrode reaction products

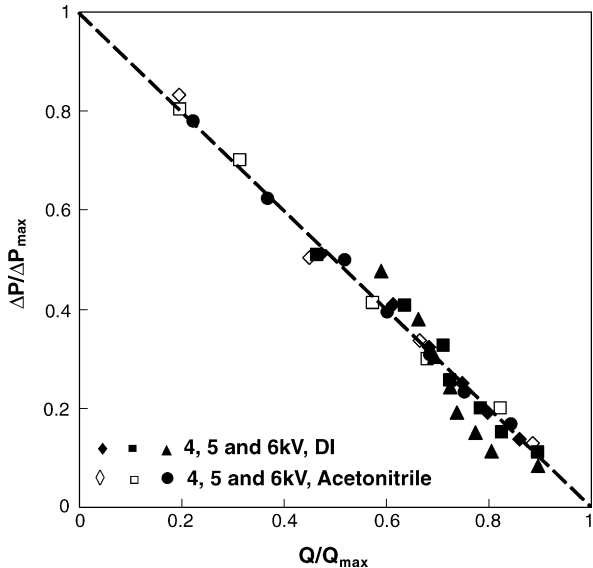


Fig. 8. Collapsed normalized pressure build-up vs. normalized flow rate where both are scaled by the measured ΔP_{\max} and Q_{\max} of the particular experiment. All data for DI water and acetonitrile for 4–6 kV are included.

like bubbles and ions are not present in our micro-pump, as they would have produce large scatters, especially at low flow rates when convection is not available to remove these products.

To obtain a more useful pump curve, we choose DI water as a reference working fluid (relative permittivity $\epsilon_r = 80.20$, viscosity $\mu = 1 \text{ cP}$ at 20°C [32] and zeta potential $\zeta = 193 \text{ mV}$) at a reference field $E_z = 0.66 \text{ kV/cm}$ for our pump capillary with a length $L = 6 \text{ cm}$ and area $A = 7850 \mu\text{m}^2$. We shall also use our monolith as a reference monolith with pore size $a = 4 \mu\text{m}$, a porosity of $\psi = 0.4$ and a nominal tortuosity of $\tau \approx 1$. We do not expect other monoliths to have very different morphologies but even other monolith morphological measures can also be included.

With these references and with the assumption that the pore size a is not much smaller than the double layer thickness λ , we can set the quantities in the parentheses of Eqs. (5) and (6) to unity (by effectively omitting the Bessel functions). All our data can then be presented as the scaled field ($E_z/E_z = 0$) as a function of $[(\Delta P/\Delta P_{\max})(L_0/L) + (Q/Q_{\max})(A_0\mu/A\mu_0)](\epsilon_r\zeta_0/\epsilon_r\zeta)$ such that the three key design parameters E_z , L and A are explicitly expressed. Our data collapse onto the linear predicted curve of Eq. (7) when L and A take on the reference values in Fig. 9. The collapse is not as good as Fig. 8, where ΔP_{\max} and Q_{\max} are measured directly. Most of the scatters are due to the 6 kV data of acetonitrile (relative permittivity $\epsilon_r = 37.5$, viscosity $\mu = 0.35 \text{ cP}$ at 20°C) [32] whose pump curve in Fig. 7 has a different slope from the other pump curves.

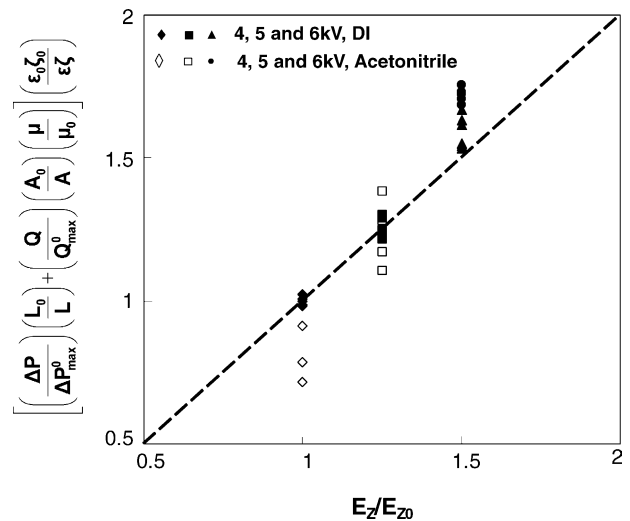


Fig. 9. Normalized field as a function of the normalized sum of pressure and flow rate. All quantities are scaled by the reference state with $a = 4 \mu\text{m}$, $L_0 = 6 \text{ cm}$, $E_z = 0.66 \text{ kV/cm}$, $A_0 = 7850 \mu\text{m}^2$, $\epsilon_r = 80$, $\mu = 1 \text{ cP}$, $\psi = 0.4$ and $\tau = 1$. These reference values correspond to our silica monolith with DI water working fluid in the capillary with a $100 \mu\text{m}$ i.d. and under a voltage of 4 kV. The reference ΔP_{\max}^0 is then 1.74 atm and the reference flow rate $Q_{\max}^0 = 1.76 \mu\text{L}/\text{min}$. The actual electric field E_z , micro-pump length L and micro-pump channel area A are the key design parameters.

The reference single-capillary pump curve of Fig. 9 for our silica monolith can be used to design silica monolith micro-pumps with dimensions different from our reference values, with a specific load and with other working fluids; provided that the double layer thickness λ is not much larger than the pore size a . The pressure P at the end of the pump is related to the flow rate Q by the load downstream. For example, an empty capillary of radius R and length l would have a flow rate driven by the micro-pump as

$$Q = \frac{\pi \Delta PR^4}{8\mu l} \quad (10)$$

A packed column would have other relationships between ΔP and Q that can be readily derived. Hence, for a specific working fluid, a specific pump geometry and a specific pressure ΔP and flow rate Q specified by the load, Fig. 9 can be used to determine the proper field E_z or voltage $V = E_z L$. One could also easily extend the approach to the case of multiple micro-pumps in parallel or multiple load channels in parallel based on the single-pump curve of Fig. 9.

5. Conclusions

Silica-based monoliths with high charge density and high porosity were successfully used for a high-pressure EO micro-pump that is only 100 μm in diameter. Since the monolith is silica-based, this pump can be used for a variety of fluids, especially for organic solvents, such as acetonitrile and methanol, without swelling problems. The average pores size is around 4 μm , which is comparable to the double layer thickness of acetonitrile or methanol. As a result, a high efficiency of 2.2% is achieved for acetonitrile. The maximum flow rates and maximum pressure generated by the pump using DI water are 2.9 $\mu\text{L}/\text{min}$ and 3 atm, respectively, at 6 kV applied voltage, without visible bubble invasion or pH change in the flow channels. A Nafion® housing design was utilized inside the cathode chamber. It has a two-fold purpose: (1) it allows current penetration by counter ions to sustain the electrolytic reaction on the cathode electrode which is outside the flow channel but prevents bubble and co-ion invasion into the pump channel and (2) it maximizes the hydrodynamic pressure created by the EO flow by eliminating flow penetration. Although we mounted this pump on a glass slide, this approach is well suited for fabrication inside micro-fluidic chip channels. The existence of a universal pump curve in Figs. 8 and 9 will facilitate the integration of this micro-pump to a large variety of micro-analysis systems.

Acknowledgements

P. Wang and H.-C. Chang were partially supported by the U.S. Army CECOM RDEC through Grant No. DAAB 07-03-3-K414. Such support does not constitute endorsement by

the U.S. Army of the views expressed in this report. Z. Chen is supported by the Center for Microfluidics and Medical Diagnostics at Notre Dame.

References

- [1] M.A. Burns, et al., An integrated microfabricated DNA analysis device, *Science* 282 (1998) 484–487.
- [2] D.S. Reichmuth, G.S. Chirica, B.J. Kirby, Increasing the performance of high pressure, high efficiency electrokinetic micropumps using zwitterionic solute additives, *Sens. Actuators B, Chem.* 92 (2003) 37–43.
- [3] H.-C. Chang, Bubble/drop transport in microchannels, in: M. Gadelhak (Ed.), *The MEMS Handbook*, CRC Press, 2001, p. 11–1.
- [4] N.T. Nguyen, X. Huang, K.C. Toh, MEMS-micropumps: a review, *J. Fluids Eng.* 124 (2002) 384–392.
- [5] D.J. Laser, J.G. Santiago, A review of micropumps, *J. Micromech. Microeng.* 14 (6) (2004) 35–64.
- [6] A. Brask, H. Bruus, J.P. Kutter, Electroosmotic pump with ion exchange membranes and a current feedback for flow control, in: Proceedings of the Micro-TAS 2003, vol. 1, Lake Tahoe, USA, 2003, pp. 223–226.
- [7] A. Brask, H. Bruus, J.P. Kutter, Long-term stability for frit-based EO pumps under varying load conditions using ion exchange membranes with controlled diffusion layer widths, in: Proceedings of the Micro-TAS 2004, vol. 2, Malm, Sweden, 2004, pp. 136–138.
- [8] B.P. Mosier, R.W. Crocker, J.L. Rognlien, K.D. Patel, High-pressure microhydraulic actuator, in: Proceedings of IMECE'03, Washington, DC, USA, 2003.
- [9] R.F. Probstein, *Physicochemical Hydrodynamics*, second ed., Wiley, New York, 1994.
- [10] V. Proetorius, B.J. Hopkins, J.D. Schieke, Electroosmosis: a new concept for high-speed liquid chromatography, *J. Chromatogr.* 99 (1974) 23–30.
- [11] F. Theeuwes, Elementary osmotic pump, *J. Pharm. Sci.* 64 (12) (1975) 1987–1991.
- [12] P.H. Paul, D.W. Arnold, D.J. Rakestraw, Electrokinetic generation of high pressures using porous microstructures, in: microTAS-98, Banff, Canada, 1998.
- [13] S. Zeng, C. Chen, J.C. Mikkelsen, J.G. Santiago, Fabrication and characterization of electrokinetic micro pumps, *Sens. Actuators B, Chem.* 79 (2001) 107–114.
- [14] S. Zeng, C.H. Chen, J.G. Santiago, J.-R. Chen, R.N. Zare, J.A. Tripp, F. Svec, J.M.J. Fréchet, Electroosmotic flow pumps with polymer frits, *Sens. Actuators B, Chem.* 82 (2002) 209–212.
- [15] C.H. Chen, J.G. Santiago, A planar electroosmotic micropump, *J. Micromech. Microeng.* 11 (2002) 672–683.
- [16] J.A. Tripp, F. Svec, J.M.J. Fréchet, S.L. Zeng, J.C. Mikkelsen, J.G. Santiago, High-pressure electroosmotic pumps based on porous polymer monoliths, *Sens. Actuators B, Chem.* 99 (2004) 66–73.
- [17] D. Lastochkin, R.H. Zhou, P. Wang, Y. Ben, H.-C. Chang, Electrokinetic micropump and micromixer design based on ac Faradaic polarization, *J. Appl. Phys.* 96 (2004) 1730–1733.
- [18] Z. Chen, T. Hobo, Chemically L-prolinamide-modified monolithic silica column for enantiomeric separation of dansyl amino acids and hydroxy acids by capillary electrochromatography and μ -high performance liquid chromatography, *Electrophoresis* 22 (2001) 3339–3346.
- [19] Z. Chen, T. Hobo, Chemically L-phenylalaninamide-modified monolithic silica column prepared by a sol-gel process for enantioseparation of dansyl amino acids by ligand exchange-capillary electrochromatography, *Anal. Chem.* 73 (2001) 3348–3357.

- [20] Z. Chen, H. Ozawa, K. Uchiyama, T. Hobo, Cyclodextrin-modified monolithic columns for resolving dansyl amino acid enantiomers and positional isomers by capillary electrochromatography, Electrophoresis 24 (2003) 2550–2558.
- [21] Z. Chen, K. Hayashi, Y. Ywasaki, R. Kurita, O. Niwa, K. Sunagawa, On-line monolithic enzyme reactor fabricated by sol-gel process for elimination of ascorbic acid while monitoring dopamine, Electroanalysis 17 (3) (2005) 231–238.
- [22] F.C. Leinweber, D. Lubda, K. Cabrera, U. Tallarek, Characterization of silica-based monoliths with bimodal pore size distribution, Anal. Chem. 74 (11) (2002) 2470–2477.
- [23] Z. Chen, P. Wang, H.-C. Chang, An electro-osmotic micro-pump based on monolithic silica for micro flow analysis and electro-sprays, Anal. Bioanal. Chem., in press.
- [24] R.J. Hunter, Zeta Potential in Colloidal Science: Principles and Applications, Academic Press, London, 1981.
- [25] C.L. Rice, R. Whitehead, Electrokinetic flow in a narrow cylindrical capillary, J. Phys. Chem. 69 (1965) 4017.
- [26] M.-S. Chun, Electrokinetic flow velocity in charged slit-like microfluidic channels with linearized Poisson–Boltzmann field, Korean J. Chem. Eng. 19 (5) (2002) 1–6.
- [27] P. Takhistov, A. Indeikina, H.-C. Chang, Electrokinetic displacement of air bubbles in microchannels, Phys. Fluids 14 (2002) 1.
- [28] S. Yao, J.G. Santiago, Porous glass electroosmotic pumps: theory, J. Colloid Interface Sci. 268 (2003) 133–142.
- [29] D. Stein, M. Kruithof, C. Dekker, Surface-charge-governed ion transport in nanofluidic channels, Phys. Rev. Lett. 93 (3) (2004), 035901-1–035901-4.
- [30] I. Nischang, U. Tallarek, Nonlinear electroosmosis in hierarchical monolithic structures, Electrophoresis 25 (2004) 2935–2945.
- [31] Y. Ben, H.-C. Chang, Nonlinear smoluchowski slip velocity and vortex generation, J. Fluid Mech. 461 (2002) 229–238.
- [32] Handbook of Chemistry and Physics, 80th ed., CRC Press, 1999–2000.

Biographies

Ping Wang is a PhD student at the Department of Chemical and Biomolecular Engineering, University of Notre Dame, USA.

Zilin Chen is a research professor at the Department of Chemical and Biomolecular Engineering, University of Notre Dame, USA. His research interests include micro-fluidics and bioanalytical chemistry.

Hsueh-Chia Chang is the Bayer professor of the Department of Chemical and Biomolecular Engineering, University of Notre Dame, USA. His research interests include micro-fluidics and complex interfacial phenomena.